Follicular dendritic cell disruption as a novel mechanism of virus-induced immunosuppression

Eleonora Melzi[a], Marco Caporale[a,b], Mara Rocchi[c], Verónica Martín[d], Virginia Gamino[e], Andrea di Provvido[b], Giuseppe Marruchella[b,f], Gary Entrican[c], Noemí Sevilla[d], and Massimo Palmarini[a,1]

[a]MRC-University of Glasgow Centre for Virus Research, Glasgow G61 1QH, Scotland; [b]Istituto Zooprofilattico Sperimentale dell'Abruzzo e Molise "G. Caporale", 64100 Teramo, Italy; [c]Moredun Research Institute, Penicuik EH26 0PZ, Scotland; [d]Centro de Investigación en Sanidad Animal (CISA-INIA), Valdeolmos-Madrid 28130, Spain; [e]Division of Pathology, Public Health and Disease Investigation, School of Veterinary Medicine, College of Medical, Veterinary and Life Sciences, University of Glasgow, Glasgow G61 1QH, Scotland; and [f]Facoltà di Medicina Veterinaria, Università di Teramo, 64100 Teramo, Italy

Edited by Rafi Ahmed, Emory University, Atlanta, GA, and approved August 15, 2016 (received for review June 22, 2016)

Arboviruses cause acute diseases that increasingly affect global health. We used bluetongue virus (BTV) and its natural sheep host to reveal a previously uncharacterized mechanism used by an arbovirus to manipulate host immunity. Our study shows that BTV, similarly to other antigens delivered through the skin, is transported rapidly via the lymph to the peripheral lymph nodes. Here, BTV infects and disrupts follicular dendritic cells, hindering B-cell division in germinal centers, which results in a delayed production of high affinity and virus neutralizing antibodies. Moreover, the humoral immune response to a second antigen is also hampered in BTV-infected animals. Thus, an arbovirus can evade the host antiviral response by inducing an acute immunosuppression. Although transient, this immunosuppression occurs at the critical early stages of infection when a delayed host humoral immune response likely affects virus systemic dissemination and the clinical outcome of disease.

arbovirus | immunosuppression | follicular dendritic cells | bluetongue | lymph node

Globalization, ecological and climate changes, and an increase in international travel have all favored the geographic expansion of numerous "arboviruses" (arthropod-borne viruses) that now pose a considerable global burden to both human and animal health (1). Similarly to other infectious agents, arboviruses induce a wide spectrum of clinical signs in the infected hosts and the clinical outcome of these infections is influenced by host- and pathogen-related factors. Consequently, the characterization of the complex interactions between virus and host are critical for better understanding the pathogenesis of arbovirus infections.

Arboviruses cause acute diseases making the study of the early stages of infection (i.e., before the onset of clinical signs) and the corresponding host responses extremely difficult in humans. Mouse models are widely used for this scope but they often fail to represent the intricate interplay between host and pathogen, which is shaped by coevolutionary adaptations. However, arboviruses naturally infect a variety of mammalian species providing opportunities to study viral infection in the natural host. For example, bluetongue virus (BTV) is the causative agent of bluetongue, one of the major infectious diseases of ruminants. Sheep affected by bluetongue show a variety of clinical signs ranging from a mild febrile illness to severe hemorrhagic disease (2). Studies on bluetongue in sheep can offer unique perspectives in understanding arbovirus pathogenesis as observations made in the naturally occurring disease can be effectively reproduced in a convenient experimental setting using the same target animal species (3).

BTV is a dsRNA virus (genus Orbivirus, family *Reoviridae*) and similarly to other arboviruses is inoculated into the skin of the host by the bite of the insect vector (*Culicoides* spp.). The skin is described as the first site of viral replication (4), and thereafter, BTV is transported to the draining lymph nodes (LNs), before disseminating further to peripheral tissues (2). The events taking place in the LNs immediately after virus arrival during bluetongue, as well as most other arboviral diseases, remain poorly defined. Peripheral LNs are the sites where the adaptive immune response to pathogens that breach the skin barrier is initiated. Different subsets of stromal cells form the tridimensional scaffolding of the LNs and are responsible for the organization of distinct functional zones that operate to maximize the interaction of B and T cells with antigen-presenting cells (5).

Although both humoral and cell-mediated immunity contribute to control viral infections, passive transfer studies have demonstrated that antibodies, unlike cytotoxic T cells, can confer full protection to BTV and prevent viremia in newly infected sheep (6). Furthermore, in BTV-infected animals, a rapid onset of the antibody response correlates with a more favorable clinical outcome (3, 7). Similar observations have been made for other arbovirus infections including those caused by West Nile virus (8), Japanese encephalitis virus (9, 10), and Crimean-Congo hemorrhagic fever virus (11). Hence, we hypothesize that the early events of infection that influence the development of humoral immunity play a key role in disease pathogenesis and its clinical outcome.

In this study, we unveil an evasion strategy used by an arbovirus to modulate the onset of the host humoral responses. We show that BTV induces an acute immunosuppression by rapidly infecting and destroying follicular dendritic cells (FDCs) and hampering the capacity of germinal centers (GCs) to produce antibodies. Our findings offer unique perspectives in understanding the pathogenesis of arbovirus infections and the mechanisms used by these viruses to overcome host immunity.

Significance

Arboviruses cause increasingly important human and veterinary diseases. Currently, there is a critical lack of understanding about the nature of arbovirus–host interactions in the lymph nodes (LNs), where the adaptive immune response initiates. We used a hemorrhagic arbovirus of sheep, bluetongue virus (BTV), to unveil the early phases of infection in the natural host. We discovered that BTV modulates the humoral immune response by rapidly infecting and destroying follicular dendritic cells (FDCs) in the host LNs. FDC destruction impairs B-cell activation and antibody production, inducing an immunosuppressive phase associated with virus spread in the animal's tissues. The novel virus evasion strategy described here provides key insights on the initiation of the immune response and the pathogenesis of arboviral diseases.

Author contributions: E.M., M.C., M.R., G.E., N.S., and M.P. designed research; E.M., M.C., V.M., V.G., A.d.P., G.M., and M.P. performed research; E.M., M.C., M.R., G.E., N.S., and M.P. analyzed data; and E.M. and M.P. wrote the paper.

The authors declare no conflict of interest.

This article is a PNAS Direct Submission.

Freely available online through the PNAS open access option.

[1]To whom correspondence should be addressed. Email: massimo.palmarini@glasgow.ac.uk.

This article contains supporting information online at www.pnas.org/lookup/suppl/doi:10.1073/pnas.1610012113/-/DCSupplemental.

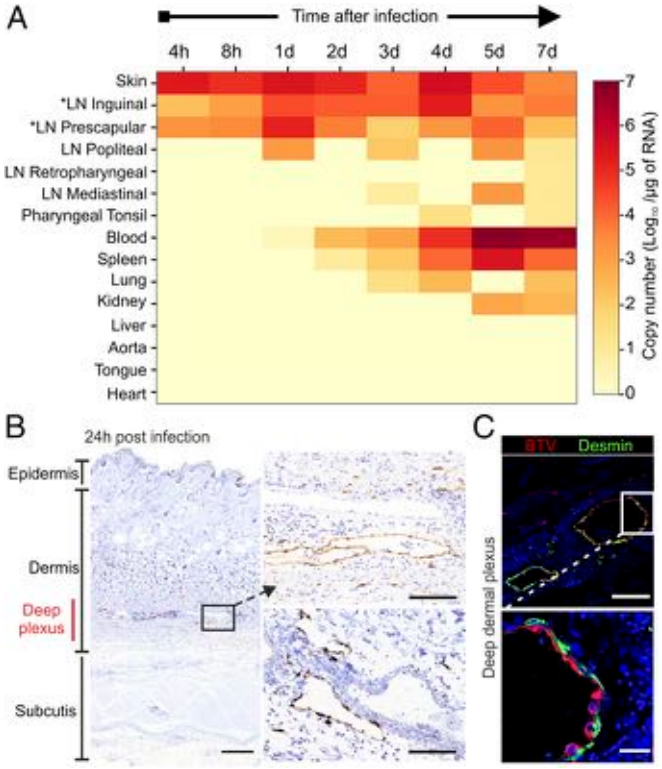

Fig. 1. Progression of BTV-8 infection in experimentally infected sheep. (*A*) Heatmap showing average BTV-8 RNA levels in tissues of experimentally infected sheep at different time points after infection. *Draining LNs. (*B*) Detection of BTV NS2 by immunohistochemistry in skin sections collected from BTV-infected sheep at 24 h postinfection (hpi). BTV NS2 (brown) was detected mainly in the lymphatic vessels of the deep dermal plexus. (Scale bars, 500 μm in left image and 100 μm in right images.) (*C*) Confocal microscopy of skin sections as in *B* showing BTV localization (NS2, red) in endothelial cells but not in desmin$^+$ pericytes (green). (*Inset*) Higher magnification of infected area. (Scale bars, 100 μm in top image and 20 μm in lower images.)

Results

BTV Dissemination in Infected Sheep. To identify the anatomic context and the kinetics in which the early stages of virus infection take place, sheep were infected intradermally with a virulent strain of BTV (BTV-8). The sheep were euthanized at different time points after infection, and BTV RNA was detected by quantitative RT-PCR (qRT-PCR; Fig. 1*A*). Viral RNA was detected in the skin, in close proximity to the inoculation sites, and in the corresponding draining LNs (inguinal and prescapular) during the initial 24 h postinfection (hpi). The levels of virus RNA were higher at 24 hpi in draining LNs and gradually decreased, whereas in blood, they started to increase significantly at 3 d postinfection (dpi) and peaked at 5 dpi. At 3 dpi, BTV-8 was also detected in mediastinal LNs, spleen, and lungs, and by 7 dpi, it was present in most of the tissues examined (Fig. 1*A*). Next, we aimed to identify the cellular targets of viral replication in the infected tissues identified by qPCR by assessing the expression of one of the nonstructural BTV proteins (NS2) by immunohistochemistry (IHC) and confocal microscopy. Considering that NS2 is a nonstructural protein, its detection within a cell can be taken as direct evidence of virus replication. In the skin, during the whole course of the experiment (Fig. 1*B*), we detected BTV-8 mainly in the endothelial cells of the deep dermal plexus in structures consistent with lymphatic, rather than blood, vessels (Fig. 1*B*). BTV-8 was not detected in pericytes (desmin$^+$), which envelope the surface of capillaries (Fig. 1*C*). Hence, cutaneous lymphatic endothelial cells represent the first target of BTV infection.

BTV Disseminates to the Draining LNs via the Lymph. The qPCR data described above suggested that there is rapid dissemination of BTV-8 to the draining LNs of the experimentally infected animals. Therefore, we used IHC to detect the areas of the LNs where the virus replicates (Fig. 2*A*). We detected BTV in the cortical area of the draining LNs as early as 4 hpi (Fig. 2*B*). As expected, virus replication was accompanied by activation of the host IFN response as demonstrated by the presence of cells expressing MX-1 (Fig. S1). At the early time points, BTV-8–infected cells were present along the subcapsular sinus (SCS) and trabecular sinuses that deepen inside the LN cortex. Presence of BTV-8 in the SCS within 4 h suggests that free virus disseminates from the skin in lymph fluids (Fig. 2*B*). Concurrently, BTV-8 was also detected within the cortical follicles in the parenchyma of the LNs. Areas of virus replication gradually expanded, and by 24 hpi, BTV-infected cells were visible in the majority of the SCS, which remained infected until 3 dpi. Thereafter, BTV-8 was detected mainly inside the follicular area (Fig. 2*B*) and only after 4 dpi in the medulla of the draining LNs in structures resembling capillary vessels.

In nondraining LNs, viral NS2 was detected by IHC only between 5 and 7 dpi in small vessels of the paracortical area and medulla, but it was not detected in the sinuses or follicles (Fig. 2*C*). These data suggest a hematogenous (rather than lymphogenous) virus dissemination to nondraining LNs. At 7 dpi, BTV-8 was also found predominantly in small capillaries of peripheral tissues (lung and kidneys) as previously described (12).

BTV was not detected in the skin and draining LNs of mock-infected sheep ($n = 8$; one sheep per time point; Fig. 2*B*). As an additional control, to exclude the possibility of detecting nonreplicating virus, sheep ($n = 2$) were inoculated with UV inactivated BTV-8. As expected, no BTV-positive cells were detected by IHC or confocal microscopy in skin or draining LNs of the inoculated sheep (Fig. S2).

BTV Infects Endothelial Cells and Macrophages in the LN sinuses. Next, we used confocal microscopy to identify the cells targeted by BTV-8. Analysis of whole transverse sections of the draining LN further supported the data obtained by IHC showing that BTV-infected cells were clearly evident in the cortical area (Fig. 3*A*). Between 4 and 48 hpi, most of the BTV-infected cells were confined inside the LN sinuses, which are delimited by a basal membrane identified with a specific staining for perlecan (13) (Fig. 3*B* and Table S1). We characterized the infected cells as JAM-A$^+$ CD83$^+$ von Willebrand factor^{low} endothelial cells lining the SCS walls (Fig. 3*C* and Table S2). These cells, frequently named "sinus lining cells," extend their processes across the SCS to enwrap sinus traversing conduits, which constitute the initial part of the intricate conduit system branching within the LN cortex (14) (Fig. 3 *C* and *D*). BTV-8 was not detected in the lumen of the conduits, which were delineated by staining for perlecan and smooth muscle actin (SMA), excluding further the possibility of the transportation of the virus within these structures (Fig. 3 *B–D* and Movie S1). BTV was also found along the trabecular sinuses up to 2 dpi, in association with a resident population of CD163$^+$ and CD169$^+$ phagocytes (Fig. 3 *E* and *F*). Contrary to the mouse, CD169$^+$ macrophages in sheep were not within the SCS but instead were found along trabecular sinuses intermingled with numerous traversing conduits sheathed with endothelial cells (Fig. 3*F*) (15).

BTV Infection of LN Follicles. The SCS forms a filter preventing the free access of large particles (≥70 kDa, 5 nm), including most of the pathogens, into the cortical area of the LNs (16, 17). Although BTV particles are too large (~80 nm) to freely access the

cortical area, we identified infected cells in the follicles very rapidly after inoculation (4–8 hpi). At these time points, we identified B cells ($BSAP^+$) as the only infected cells in some follicles, whereas in others, we detected BTV-8 both in B cells and in cells with spindle morphology (Fig. 3*G*). These data suggest a temporal sequence in which B cells are infected before the spindle cells. Follicular B cells have the capacity to sample antigens from the SCS area and transport them to FDCs or to T cells in the paracortex, at the limit with the follicular area (15). Approximately 70% of the infected B cells were visualized in close contact with the infected SCS or just beneath it, in the area of the follicle closer to the capsule (Fig. 3*H*). These data indicate the subcapsular area as the most likely site of infection for B cells. At 24 hpi, BTV-infected B cells were no longer detectable in the cortical area, whereas infected spindle cells could be detected up to 3–4 dpi. BTV NS2 was not detected in $CD3^+$ T cells, and only in extremely rare occasions we identified infected dendritic cells (defined as $CD208^+$ MHC-II^+ $fascin^{high}$ with dendritic morphology) in the paracortical area of the LNs (Fig. S3).

BTV Infects and Disrupts FDCs and Marginal Reticular Cells. To identify the spindle cells infected by BTV in the follicle, we first characterized the stromal cells composing the sheep LNs (Fig. 4 *A*–*C*). Aside for some minor differences with what has already been described in the mouse (5), we were able to identify (*i*) fibroblastic reticular cells (FRCs) in the paracortical and medullar area of the LN (Fig. 4*A*), (*ii*) FDCs inside the follicles (Fig. 4 *A*–*C*, Fig. S4, and Table S2), (*iii*) reticular cells in the dark zone of the follicles (Fig. 4*B*), and a population of cells corresponding to (*iv*) marginal reticular cells (MRCs) just underneath the SCS in the outer edges of the follicles (Fig. 4*C* and Table S2).

We could determine the identity of the BTV-8–infected spindle cells as MRC, dark zone reticular cells, and FDCs (Fig. 4 *D* and *E* and Movie S2) constituting the stromal cells supporting the follicle. We did not detect BTV in $desmin^+$ cells (FRCs) in the paracortical area of the LNs nor in high endothelial venules or perycites. Over time, the reticular network of cells present in the follicles of infected sheep adopted an increasingly disrupted appearance both in the light (FDCs) (Fig. 5*A*) and in the dark zone (reticular cells) (Fig. 5*B*). Indeed, in some of the follicles, it was not possible to detect any FDCs. As expected, mock-infected controls always displayed FDCs in LN follicles. In infected sheep, numerous apoptotic cells, characterized by high levels of expression of caspase-3, were also observed in the subcapsular and trabecular sinuses and inside the follicles between 8 and 24 hpi. Activated caspase-3 was not present in the cortical area of mock-infected controls or in sheep infected with UV-inactivated BTV-8, indicating that apoptosis was a consequence of virus replication (Fig. S5).

BTV Infection Hampers Centroblast Division. FDC are necessary for the recruitment of B cells into follicles and the development of GCs (18). GCs present a cluster of immature B cells, called centroblasts, that undergo somatic hypermutation in the dark zone of the follicle (19).

Despite the relative lack of FDC in BTV-infected draining LNs, B cells were maintained in follicular structures throughout the duration of the experiment (4 hpi to 7 dpi). However, follicles of BTV-8–infected animals presented a less compact structure, with numerous scattered B cells, compared with mock-infected controls (Fig. 6*A*). Importantly, we observed a rapid shutdown of B-cell division (assessed by lack of $Ki67^+$ B cells) by 4 hpi in follicles of draining LNs collected from BTV-8–infected animals (Fig. 6 *B*–*D*). At 4 hpi, follicles localized near the SCS presented BTV-8–infected FDCs and displayed few dividing cells (Fig. 6 *B, i* and ii). On the contrary, follicles localized deeper in the cortex were not reached by the virus and preserved a normal

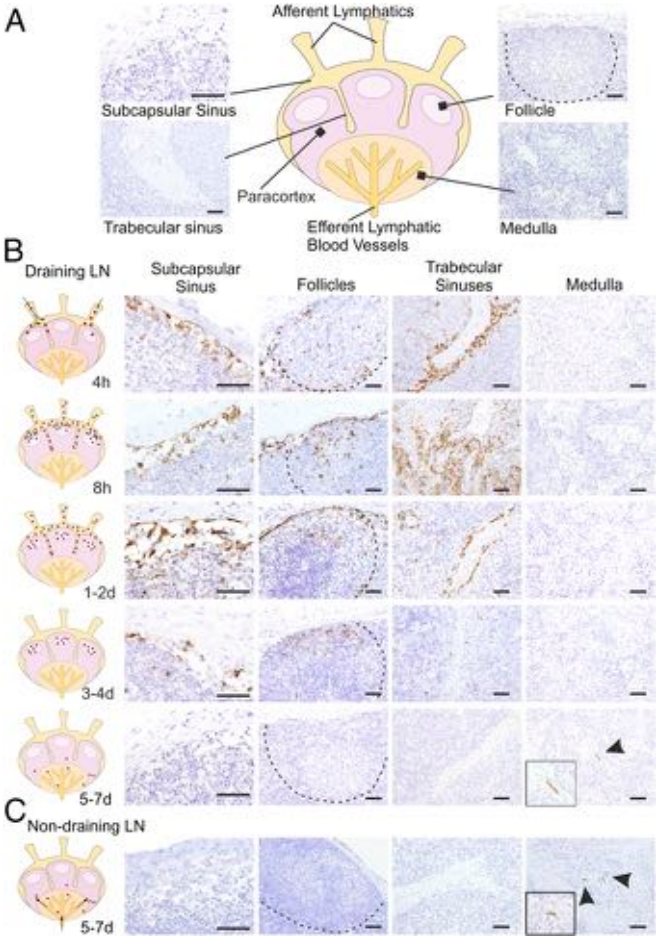

Fig. 2. Progression of BTV infection in the LNs. (*A*) Schematic diagram of a LN with representative micrographs of sections collected from mock-infected sheep used as negative control for the detection of BTV NS2 by immunohistochemistry. (*B*) Detection of BTV NS2 by immunohistochemistry in draining LNs (inguinal and prescapular) of BTV-8–infected animals collected at different times after infection. BTV-infected areas and likely infection routes are schematically depicted in the diagrams on the left. See also Fig. S1. (*C*) Detection of BTV NS2 in nondraining LNs by immunohistochemistry as above at 7 dpi. In these sites BTV NS2 is visible only in capillary vessels of the medullary cords. (Scale bars, 50 μm.)

structure with FDC in the light zone and centroblasts in division in the dark zone (Fig. 6 *B*, *iii*). To determine whether there was a correlation between virus replication and block of B-cell division, we assessed the presence of $Ki67^+$ B cells in infected and uninfected follicles (Fig. 6 *B*–*D*), considering that in the same LN section it was possible to observe both BTV-infected and -uninfected areas (Fig. 6*B*). The percentage of BTV-8–infected follicles containing clusters of dividing B cells was 12.5% at 8 hpi and decreased to 4–8% between 1 and 3 dpi (Fig. 6*C*). In contrast, in follicles where BTV-8 was not detected, we observed that on average 50% of follicles contained clusters of dividing B cells up to 2 dpi that decreased to ∼40% at 3 dpi (Fig. 6 *C* and *D*). At later time points, as the virus began to be cleared from the LNs, very few follicles presented BTV-8–infected cells, and therefore, we could not carry out an accurate comparison between infected and uninfected follicles.

Division of B Cells in GCs Resumes More Rapidly in Sheep Infected with an Attenuated BTV-8 Strain ($BTV8_H$). The data above suggest that BTV-8 infection and disruption of FDC induce shut down of B-cell division in preexisting GCs. Hence, we next used an attenuated strain of BTV-8 ($BTV8_H$) (20) to assess if this shutdown was

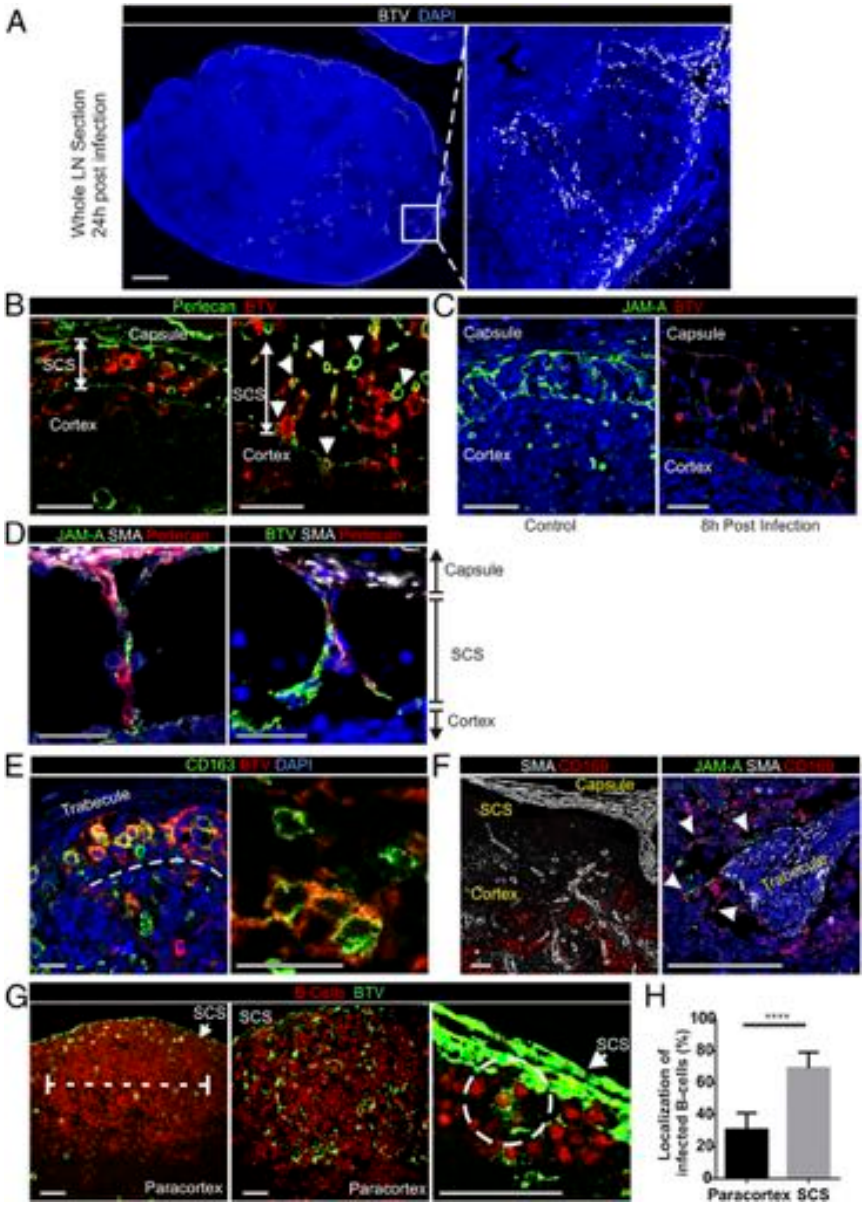

Fig. 3. BTV infection of subcapsular and trabecular sinuses leads to infection of follicles in LNs. (*A*) Confocal microscopy (stitched image of confocal tiles) of a whole sheep draining LN section collected from a BTV-8–infected sheep at 24 hpi. BTV-infected cells are shown in white, whereas nuclei are stained with DAPI (blue). Note the localization of the virus along the subcapsular area. Inset of a follicle at higher magnification is shown in the right panel. (Scale bar, 1 mm.) (*B*) Confocal images of LN sections (as in *A*) stained for BTV NS2 (red). Perlecan (green) identifies the basal membrane of the SCS. Infected cells reside inside the sinus. Arrows indicate transverse section of infected conduits delimited by perlecan. Note that BTV is not detected inside the conduits but only in the surrounding cells. (Scale bars, 50 μm.) (*C*) Confocal images of LN sections stained for JAM-A (green, sinus lining cells) and BTV NS2 (red) showing virus infection of lymphatic endothelial cells lining the sinus and traversing conduits. (Scale bars, 50 μm.) (*D*) Confocal images showing the structure of the sinus traversing conduits (Movie S1) in LN sections. Sections were stained for JAM-A (green in the left image) or BTV NS2 (green in the right image), SMA (white), and perlecan (red). (Scale bars, 25 μm.) (*E*) Confocal images of trabecular sinuses showing BTV infection of $CD163^+$ macrophages. LN sections were stained for BTV NS2 (red) and CD163 (green). (Scale bars, 25 μm.) See also Fig. S3. (*F*) Confocal images of the cortical area showing the localization of $CD169^+$ macrophages (red) along trabecular sinuses. LN capsule and trabecular structures are stained with SMA (white). (*Right*) Higher-magnification images show the localization of $CD169^+$ macrophages (red) along the trabecules (SMA, white) intermingled with JAM-A^+ endothelial cells (green). (Scale bars, 75 μm.) (*G*) Confocal image of LN section collected 8 hpi showing two different patterns of BTV infection in the follicle. (*Left*) Only B cells are infected with BTV. (*Center*) BTV NS2 is detectable both in B cells and in spindle-shaped cells. (*Right*) Higher-magnification image of the SCS area shows infected B cells in close contact with the SCS. Sections were stained for B cells (BSAP, red) and BTV NS2 (green). (Scale bars, 50 μm.) (*H*) Localization of BTV-8–infected B cells in the LN follicles at 8 hpi. Follicles were divided in two equal parts: one facing the SCS and one facing the paracortical area. The number of infected B cells in the two areas was counted in six LNs from three different animals (****$P < 0.0001$ by Mann-Whitney *U* test).

correlated with virus pathogenicity. We followed the progression of $BTV8_H$ by euthanizing sheep at different time points after infection and assessed virus replication by qRT-PCR, IHC, and confocal microscopy (Fig. S6). $BTV8_H$ was found to infect skin and draining LN but was not detected in blood and peripheral tissues (Fig. S6*A*). More specifically, $BTV8_H$ was detected in similar locations and cells of the draining LNs (including FDCs) as in BTV-8-infected animals (Fig. S6 *B* and *C*).

Next, we compared the proportion of GCs (identified by clusters of $Ki67^+$ B cells) relative to the number of primary

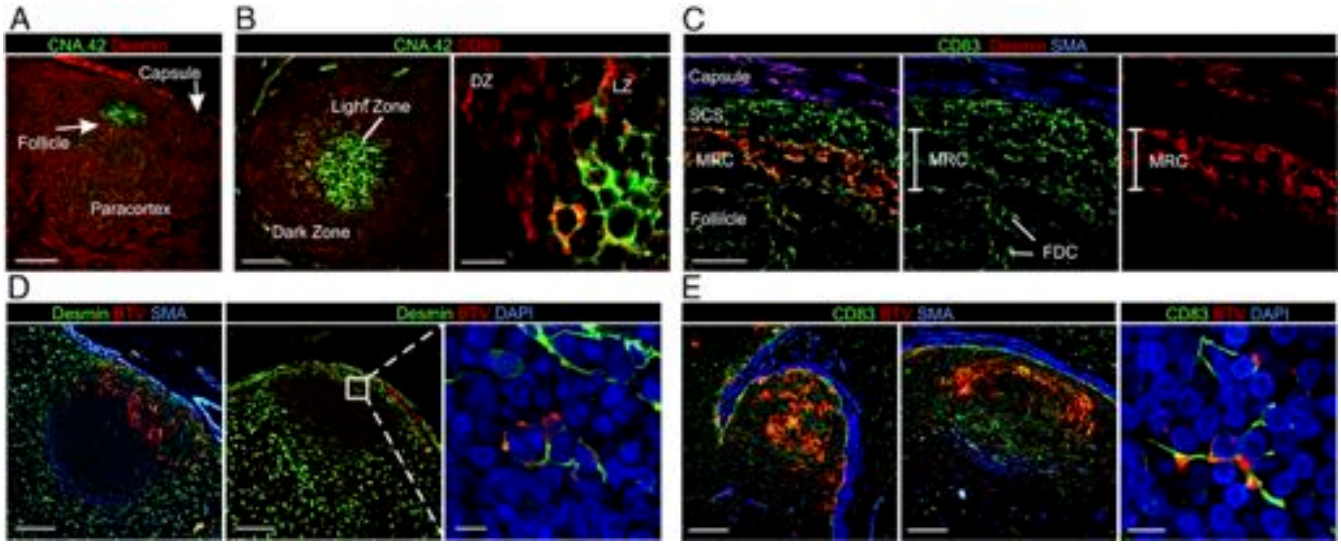

Fig. 4. BTV targets stromal cells in the follicles of the draining LNs. (*A*) Confocal image of a LN section collected from a mock-infected sheep showing the identification of desmin$^+$ FRCs (red) in the paracortex. FRCs are absent in the follicles, whereas FDCs can be identified by expression of CNA.42 (green). (Scale bar, 150 μm.) (*B*) Images as in *A*. In the follicle, the network of reticular cells in the dark zone (DZ) is labeled with CD83 (red), whereas CNA.42$^+$ FDCs are located in the light zone (LZ). (Scale bars, 75 μm in left image and 15 μm in right image.) See also Fig. S4. (*C*) Images as above showing the identification of the stromal cells populations in the subcapsular area of the LN. MRCs reside between the SCS and the follicle and are labeled with desmin (red) and CD83 (green). MRCs are adjacent to the lymphatic endothelial cells of the SCS on one side and the FDCs on the other side. All of the three cell types can be labeled with CD83. The LN capsule can be defined by desmin and SMA expression. (Scale bars, 40 μm.) (*D*) Representative confocal images of LN sections collected from BTV-8–infected sheep. BTV NS2 (red) is expressed in MRCs (desmin$^+$, green). (*Inset*) Higher magnification of infected MRCs. (Scale bars, 100 μm in left images and 10 μm in inset.) (*E*) Representative confocal images of LN sections from BTV-8–infected sheep showing infection of CD83$^+$ FDCs. (*Left*) Sections stained for BTV NS2 (red), CD83 (green), and SMA (blue). (*Right*) Sections stained for CD83 (green) and BTV NS2 (red), whereas nuclei are stained with DAPI (blue) (Movie S2). (Scale bars, 100 μm in left images and 10 μm in right image.)

follicles present in sequential LN sections collected at different times after infection from sheep infected with either BTV8$_H$, BTV-8, or mock-infected (Fig. 7*A*). Between 10% and 24% of follicles contained clusters of Ki67$^+$ B cells in LN collected at 3 and 4 dpi in sheep infected with either BTV-8 or attenuated BTV8$_H$. In LNs from mock-infected sheep, GCs represented around 70% of the total number of follicles throughout the duration of the experiment (Fig. 7*A*). Interestingly, at 7 dpi, in BTV8$_H$ but not in BTV-8–infected animals, the presence of GCs was reestablished to normal levels (Fig. 7 *A* and *B*). Hence, the extent of the cellular damage induced by BTV8$_H$ is reduced compared with BTV-8, resulting in an earlier recovery of B-cell division in animals infected with the attenuated virus.

Antibody Response Differs in Sheep Infected with Virulent or Attenuated BTV-8. Our data indicated that BTV led to the suppression of GCs, which are the site of affinity-based selection that generates high affinity antibodies and memory B cells (19). We hypothesized that BTV could also affect the initiation of the host humoral immune response. Therefore, we characterized the antibody responses over 21 d in sheep infected with either BTV-8 ($n = 3$) or BTV8$_H$ ($n = 5$) (Fig. 7 *C*–*E*).

Animals infected with BTV-8 developed a prolonged viremia, detectable throughout the course of the experiment, and showed an increase in body temperature between 5 and 7 dpi, whereas BTV8$_H$ induced neither fever nor viremia (Fig. 7 *C* and *D*). No significant differences were evident in the levels of IgM specific for the major core protein of BTV (VP7) between the two groups of infected animals (Fig. 7*E*). However, at 7 dpi, BTV8$_H$-infected sheep produced significantly higher titers of both anti-BTV VP7 IgG and virus neutralizing antibodies compared with BTV-8–infected sheep ($P \leq 0.05$ in both cases; Fig. 7*E*). These differences were transitory, and by 14 dpi, the two groups of experimentally infected sheep showed similar levels of both anti-VP7 IgGs and BTV-8 neutralizing antibodies (Fig. 7*E*). In both BTV-8– and BTV8$_H$-infected sheep, antibody (IgG) avidity increased over time. However, BTV8$_H$-infected animals consistently showed IgGs of higher avidity toward VP7 at 7, 14, and 21 dpi ($P \leq 0.05$) compared with BTV-8–infected sheep (Fig. 7*E*).

BTV Infection Induces an Acute Immunosuppression. We showed above that BTV-8 hampered specific B-cell responses to the virus. Therefore, we hypothesized that BTV could also be the cause of a more generalized immunosuppression by affecting GCs function. To test this hypothesis, we assessed the ability of BTV-8–infected sheep to elicit a humoral response to an exogenous antigen. Sheep were infected with BTV-8 and then immunized with ovalbumin (OVA) at either 1 ($n = 5$) or 3 dpi ($n = 5$). A control group of sheep ($n = 5$) was immunized with OVA without prior BTV infection (Fig. 8*A*). Sheep immunized with OVA at 24 h following BTV inoculation demonstrated a significant reduction in circulating OVA-specific IgM and IgG titers at day 7 ($P < 0.01$) and day 14 (IgM $P < 0.01$; IgG $P < 0.05$) after immunization compared with uninfected controls (Fig. 8*B*). Strikingly, the formation of OVA-specific antibody secreting cells (ASCs) was almost completely ablated in BTV-infected animals ($P < 0.01$), suggesting that the humoral immune response during this critical stage of infection is compromised. On the other hand, animals immunized with OVA 72 h after BTV infection exhibited a less substantial decrease in the levels of OVA-specific antibodies and ASCs compared with uninfected controls (Fig. 8*B*). These data indicate that the inability of BTV-infected sheep to produce OVA-specific antibodies is temporary.

Discussion

After gaining entry into the mammalian host, arboviruses need to overcome host antiviral responses to replicate abundantly in susceptible cells and produce sufficiently high titers in the bloodstream to be infectious for competent biting insects. In this study, we characterized a strategy used by an arbovirus to

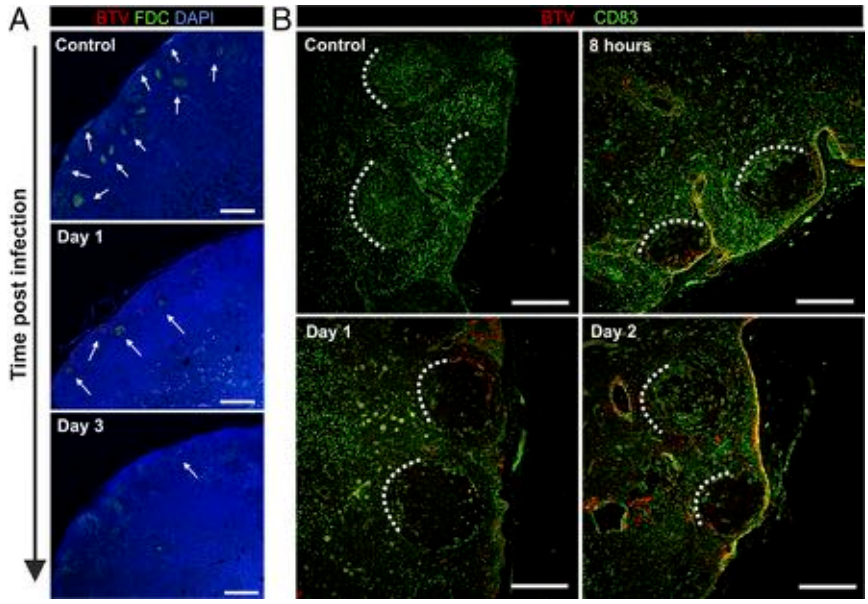

Fig. 5. BTV disrupts the FDC network in the light and dark zones of the follicles. (*A*) Confocal tile scan images of LN sections collected from BTV-8–infected sheep showing the presence of FDCs in the cortical area at different time points after infection. Sections were stained for BTV NS2 (red), CNA.42 (FDC, green), and DAPI (blue). Arrows indicate recognizable follicles. (Scale bars, 1 mm.) (*B*) Confocal images of LN sections from BTV-8–infected sheep (at the indicated time after infection) showing the progressive disruption of the $CD83^+$ reticular cell network normally present in uninfected follicles. Sections are stained for BTV NS2 (red) and CD83 (green). Dashed lines help to identify follicles. (Scale bars, 300 μm.) See also Fig. S5.

modulate host immunity, and we demonstrate how the early stages of infection can influence the severity of disease. In particular, we showed that BTV, one of the major arboviruses affecting ruminants, infects and disrupts FDCs in the peripheral LNs, inducing subversion of the host humoral immune response and acute immunosuppression.

FDCs are long interdigitating cells of stromal origin residing in the B-cell follicles. They promote the formation and maintenance of GCs where B cells differentiate into memory cells or antibody-producing plasma cells (19, 21). FDCs are considered long-lasting cells that have the unique ability to retain unprocessed opsonized antigens for a long period, supporting antibody class switching and affinity maturation (22). For these characteristics, FDCs are exploited by pathogens, such as prion proteins and HIV, to persist undisturbed into the host (23–26). It has been demonstrated that the experimental abrogation of the FDC network can rapidly abolish the normal follicular structures (27). In this study we show rapid disruption of the FDC network as a consequence of an acute viral infection. Our data are consistent with a direct cytopathic effect of BTV on FDCs, given the rapidity of their depletion (between 4 and 24 hpi in our experimental model) and the abundant presence of BTV antigens in FDCs in concomitance with the detection of apoptotic cells in the follicles.

After FDC depletion, we observed a loss of follicles organization and a sudden shutdown of centroblasts division hampering the process of somatic hypermutation in the dark zone of the GC, as confirmed by the detection of low avidity antibodies in infected sheep. These findings indicate a delay in the antibody affinity maturation that was maintained over an observation period of 28 d, suggesting that an acute damage at FDC can have long-term repercussions even after the recovery of the GCs functionality. We cannot exclude that other factors, besides the disruption of FDCs, may contribute to the immune dysregulation observed in BTV-infected animals. However, the structural and functional defects of the immune system of sheep during the early stages of BTV infection resemble those described in mouse models where FDC were artificially ablated (18, 28, 29).

Our data also indicate that the severity of the BTV-induced immunosuppression is associated with virus virulence and the clinical outcome of infection. Using virulent and attenuated strains of BTV-8, we identified a correlation between the recovery of GCs in infected animals and the production of high affinity and neutralizing antibodies. $BTV8_H$ possesses attenuating mutations in several viral proteins hampering optimal replication both in vitro in primary cells and in vivo in sheep and $IFNAR^{-/-}$ mice (20). Hence, it is most likely that the phenotype observed in BTV-infected sheep is directly proportional to the extent of the damage induced by the virus to the FDC network, although other factors may play a role. Several elements affect the variable clinical outcome of BTV infection (3). The observations made in this study suggest that BTV virulence is, at least in some cases, due to the capacity of the virus to damage the FDC network. In turn, FDC depletion will affect the prompt development of a neutralizing antibody response during the early stages of infection that is likely to hinder virus dissemination to peripheral tissues and virus-induced pathology.

The route of BTV inoculation has been found to affect the clinical outcome of experimental BTV infection. In this study, we used intradermal inoculation to mimic insect bites and begin viral infection in the natural anatomic compartment of the host. Interestingly, experimental infection of sheep by i.v. inoculation often fails to induce clinical disease (30). This observation, in addition to the data presented in this study, suggests that virus replication in draining LNs is critical for virus pathogenesis. Indeed, we showed that BTV replication in FDC occurs only in LNs draining the site of virus inoculation but not in other peripheral LNs. The latter are reached through blood dissemination by BTV at later stages of infection and in these LNs the virus replicates mainly in endothelial cells of the capillaries of the paracortex and medulla. Therefore, it appears that BTV needs to be transported by the lymphatic system to access the cortical area of the LN and infect the follicular region. Hence, inoculation through the insect bite in the skin is key to enabling the virus to reach the FDC compartment, shutdown GCs, and induce immunosuppression.

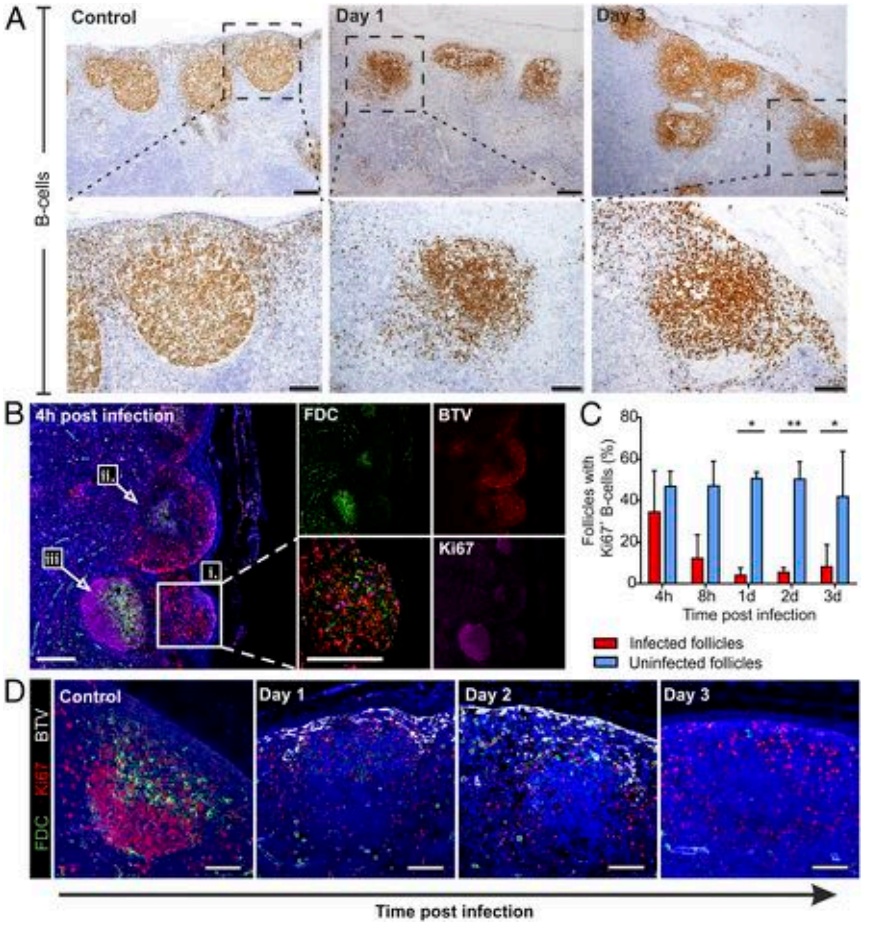

Fig. 6. FDC infection alters B-cell localization and halts centroblasts division. (*A*) Immunohistochemistry of LN sections collected from uninfected controls and BTV-infected sheep at 1 and 3 dpi. Higher-magnification micrographs of individual follicles are shown in the bottom row. B cells are stained with BSAP (brown). [Scale bars, 200 μm (top row) or 100 μm (bottom row).] (*B*) Representative confocal images of LN sections collected from BTV-infected sheep at 4 hpi showing the progression of virus replication in the cortical area. BTV NS2 (red), CNA.42 (green), and Ki67 (purple) staining is shown. Nuclei are stained with DAPI (blue). Note the presence of (*i*) an infected follicle with few Ki67$^+$ cells (*Inset* and higher magnification), (*ii*) a partially infected follicle showing disruption of the FDC network, and (*iii*) an uninfected follicle. (Scale bars, 200 μm.) (*C*) Graph showing the percentage of BTV-infected follicles containing dividing B cells (Ki67$^+$) in comparison with uninfected follicles within the same section. Sequential LN sections were stained for B cells, BTV NS2, and Ki67. The total number of follicles per section was quantified (range = 44–254 follicles per section) in a minimum of three draining LN per each time point. Histograms represent mean ± SD (*$P \leq 0.05$, **$P < 0.01$, paired *t* test). (*D*) Representative confocal images of LN sections collected from BTV-infected sheep at different time points after infection showing the shutdown of centroblasts division in infected follicles up to 3 dpi. Sections were stained for BTV NS2 (white), CNA.42 (green), and Ki67 (red). Nuclei are stained with DAPI (blue). (Scale bars, 100 μm.)

As for other arboviruses, LNs have been recognized as early sites of BTV replication (31, 32), but the cells infected by the virus in these organs had not been characterized before. It has been suggested that dendritic cells were the main responsible of supporting LN infection, given their involvement in the transport of BTV from the skin to the LN (33). However, our data do not provide evidence of a substantial infection of dendritic cells in the LN. Furthermore, the rapid localization of BTV in the SCS of the draining LN (4 hpi) is consistent with the delivery of free virus with lymphatic fluids rather than dendritic cells carriage.

It is interesting to note how BTV reaches the FDCs, considering that they are located at the center of the follicle and physically isolated in a protected environment to prevent the removal of opsonized antigens. Two mechanisms have been described that can account for rapid antigen delivery to FDC: (*i*) small antigens <70 kDa (~5 nm) have free access to a system of conduits wrapped by stromal cells that opens in the SCS and branches in both the T- and B-cell areas (16, 34), whereas (*ii*) larger antigens are acquired by follicular B cells from SCS macrophages and shuttled to FDCs (15, 35, 36). Both systems seem to rely on the presence of opsonizing antibodies. Nevertheless, we showed that BTV rapidly colocalizes with B cells and FDCs in naïve animals, without the requirement of preexisting antibodies or cognate B cells. BTV infectious particles are too large (~75 nm) to directly access the conduits; however, we identified numerous infected sinus lining cells and MRCs that constitute the walls of the conduits leading to the follicles. It is therefore likely that the virus spread by contiguity along these cells until reaching FDCs. Alternatively, infected motile B cells could also contribute to carrying virus toward the center of the follicles during their migrations and scanning for antigens, given that we identified BTV-8–infected B cells underneath the SCS before FDC infection.

MRCs have been recently identified as precursors of LN FDCs in the mouse (37). Indeed, we could label (*i*) sinus lining cells, (*ii*) MRCs, and (*iii*) FDCs with the same marker (CD83). Curiously, these cells were all infected by BTV, whereas we never observed BTV replication in the stromal cells of the T-cell area (which do not express CD83) or in pericytes surrounding the high endothelial venules, which have been proposed to be the progenitor of FDC in the mouse spleen (38). The origin of LN FDC is still debated; however, the data shown here might indirectly suggest that because these different stromal cell

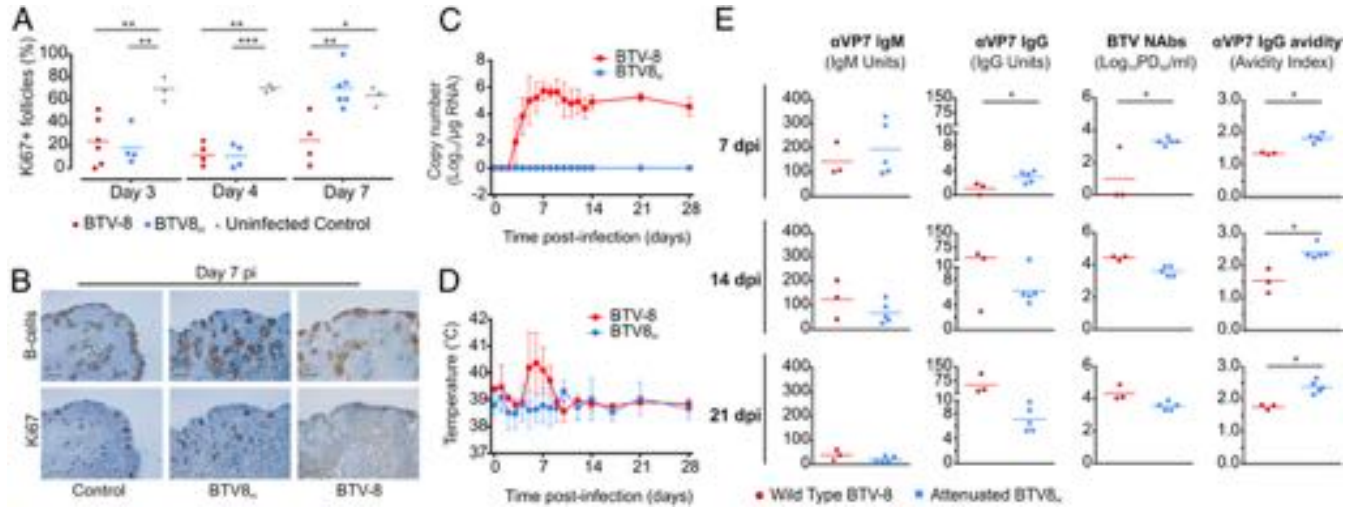

Fig. 7. Sheep infected with $BTV8_H$ display early recovery of GCs and faster production of neutralizing antibodies compared with sheep infected with BTV-8. (*A*) Percentage of follicles displaying clusters of $Ki67^+$ cells in draining LNs of sheep infected with BTV-8, $BTV8_H$, or uninfected controls at 3, 4, and 7 dpi. The number of follicles and Ki67 clusters were quantified in sequential sections stained either for BSAP (B cells) or Ki67 (*$P \leq 0.05$; **$P \leq 0.01$; ***$P \leq 0.001$ by one-way ANOVA). Bars represent the average values. (*B*) Representative micrographs of sequential sections collected from LNs of sheep as in *A* and stained for B cells (BSAP) and Ki67 at 7 dpi. Few GCs are visible in draining LN sections collected from sheep infected with BTV-8. (*C* and *D*) Viremia and rectal temperature (average ± SD) in sheep infected with either BTV-8 ($n = 3$) or $BTV8_H$ ($n = 5$). Animals were monitored for 28 dpi. See also Fig. S6. (*E*) Graphs showing the quantification of anti-BTV VP7 IgG and IgM, serum neutralization titer (NAbs), and anti-VP7 IgG avidity as assessed by specific ELISAs and microneutralization assays in BTV-8– and $BTV8_H$-infected sheep. Each dot represents values for an individual sheep, whereas bars represent the average values (*$P \leq 0.05$ and **$P \leq 0.01$ by Mann-Whitney *U* test).

populations are all targeted by BTV (an endotheliotropic virus), they could potentially share the same endothelial origin. It will be important to evaluate whether arboviruses that cause hemorrhagic fevers and with a tropism for endothelial cells, such as Rift valley fever virus, yellow fever virus, Crimean-Congo hemorrhagic fever, and others, may all target FDCs in the early stages of infection and cause immunosuppression.

In this study, we dissected the kinetics and tropism of an arbovirus during the early stages of infection in its natural host. Mouse models of arbovirus infection are limited by the fact that they generally lack a fully competent immune system to permit virus replication. The experimental infection of the natural host has the advantage to recapitulate the whole immune pathological events that lead to disease. Moreover, the sheep included in our experiments have been naturally exposed to environmental pathogens and commensals, which shape the immune system of the host. Indeed, in the LNs of these sheep we found the presence of numerous GCs preceding infection with BTV. GCs are generally missing in laboratory mice kept in clean animal facilities. Therefore, the virus-induced lesions that we described in this study would have been difficult to observe in conventional murine models. Furthermore, in the mouse, lymphborne viruses can be sampled by a layer of $CD169^+$ macrophages in the SCS (15). In sheep, despite the presence of $CD169^+$ macrophages in the trabecular sinuses, we could not identify a homologous population of phagocytes in the subcapsular area, where instead endothelial sinus lining cells (39) were the main cell population infected by BTV. Mouse SCS macrophages are thought to be key in the initiation of the immune response, as they can capture and present antigens to B cells (15, 35). The disruption of the SCS macrophage layer has been associated with immunosuppression following infection and inflammation (40, 41); however, the lack of these cells in the aforementioned position in sheep raises questions about the role of these cells in other mammalian species.

Here, we propose a different immunosuppressive mechanism, independent from the presence of SCS macrophages, based on the alteration that we have observed in FDCs in the course of BTV infection. Our data show that BTV infection impairs the function of GCs to respond to a subsequent antigenic stimulus. Indeed, we found the levels and avidity of serum IgG and the number of ASCs toward a second antigen (OVA) to be significantly lower in the presence of BTV. Interestingly, the lack of FDCs induced also a delay in the IgM response against OVA, indicating that FDCs can influence B-cell responses at various levels of maturation as suggested by previous in vitro studies (22). The subversion of the host humoral immune response is transient, and after a short time

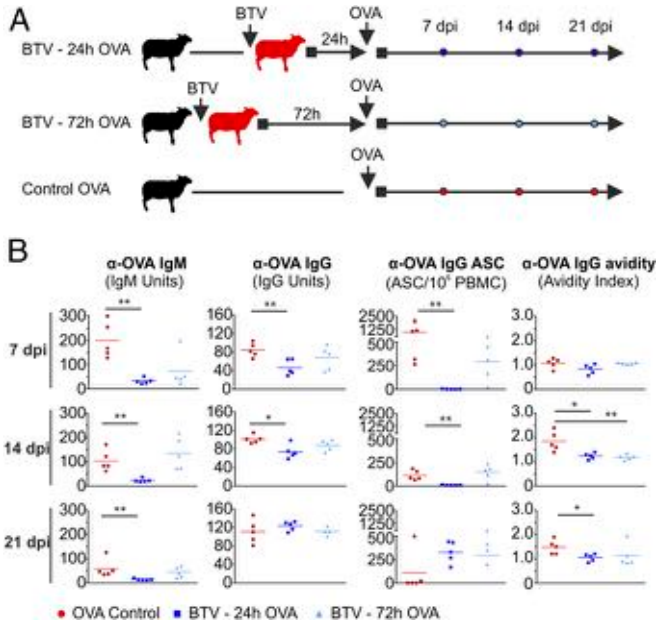

Fig. 8. BTV infection induces a transient immunosuppression. (*A*) Experimental design. Sheep were divided into three groups ($n = 5$ per group). All groups were immunized with OVA. Two of the three groups were previously infected with BTV either 24 or 72 h before OVA immunization. (*B*) Titers of OVA-specific IgM, IgG, ASCs, and IgG avidity at different times after immunization. Each dot represents values for an individual sheep, and bars represent the average values (*$P \leq 0.05$ and **$P \leq 0.01$ by Mann-Whitney *U* test).

frame (3 d), infected animals become responsive to newly administered exogenous antigen while still showing a delay in the affinity maturation process, which is therefore the last function of the GCs to recover after a FDC insult. Although transient, this immunosuppression occurs at a key stage of infection, during which delayed antibody production is likely to affect the systemic spread of the virus and the clinical course of the disease.

In conclusion, in the present study, we identified how a vector-borne virus can subvert the host immune response by inducing a temporary immunosuppression characterized by impaired GCs formation and delayed antibody affinity maturation. The identification of this process opens a way to understanding previously uncharacterized mechanisms of arbovirus–host interactions and pathogenesis. Virus infection of FDCs also offers new avenues in understanding the origin of these cells and the key role they play in the biology of GCs.

Materials and Methods

Details of all experimental procedures can be found in *SI Materials and Methods*.

Cells. Vero, BHK-21, BSR (a clone of BHK-21), and ovine choroid plexus cells (CPt-Tert) were cultured as described before (3, 42).

Viruses. $BTV8_{NET2006}$ (referred simply as BTV-8 in this study) and the attenuated $BTV8_H$ strain have been previously described (3, 20). Virus titers were assessed by standard plaque assays and endpoint dilution assays as described previously (3).

In Vivo Experiments. Animal experiments were carried out at the Istituto Zooprofilattico Sperimentale dell'Abruzzo e Molise "G. Caporale" (Teramo, Italy) and at the Centro de Investigación en Sanidad Animal (Madrid, Spain) in accordance with locally and nationally approved protocols regulating animal experimental use over a period of ∼4 y [protocol numbers 7440; 11427; 12301 (in Teramo) and 10/142792.9/12, CBS2012/06 and PROEX 228/14 (in Madrid)].

Study 1. To follow the temporal dissemination of the infection in the natural host, Sardinian breed sheep were intradermally (ID) infected with 2×10^6 PFU of BTV-8 ($n = 23$). Control animals ($n = 8$) were mock infected with cell culture supernatant. Two additional control sheep were inoculated with 2×10^6 PFU of UV-inactivated BTV-8. Animals were monitored throughout the course of the experiment. Blood samples were collected to detect viremia. Sheep were euthanized at the following time points after infection: 4, 8, 24, 48, 72, 96, 120, and 168 hpi ($n = 3$ per time point with the exception of 96 hpi where $n = 2$). Tissues were collected and either fixed in formalin or zinc salts solution (BD Biosciences) and embedded in paraffin for histological studies or stored at −20 °C in RNAlater (Thermo Fisher) for viral nucleic acid detection.

Study 2. To evaluate the LN responses to an attenuated BTV strain, 13 sheep were infected with $BTV8_H$. Animals were euthanized at 8, 24, 48, 72, 96 ($n = 2$), and 168 hpi ($n = 3$).

Study 3. Sheep were inoculated with BTV-8 ($n = 3$) or $BTV8_H$ ($n = 5$) and monitored for 28 d. Blood and serum samples were collected at different times after infection.

Study 4. Two groups of sheep ($n = 5$ each group) were inoculated with BTV-8 and then immunized with 20 mg ovalbumin (OVA) at 24 or 72 hpi, respectively, to compare the antibody response against a second antigen during the course of BTV infection. A third group of sheep ($n = 5$) was immunized with OVA (20 mg) with no prior BTV infection and was used as a control. Blood and serum samples were taken at various time points after OVA immunization.

RNA Extraction and qRT-PCR. RNA extraction and qRT-PCR were carried as described previously (3). BTV genome copy number was expressed as $\log_{10}$ per microgram total RNA and was derived using a standard curve generated from the amplification of in vitro transcribed synthetic BTV segment 5 RNA.

Immunohistochemistry and Immunofluorescence. Tissue sections were deparaffinized and rehydrated using standard procedures. Antibodies used and cells targeted are shown in Tables S1 and S2. Immunohistochemistry was performed using Dako EnVision kit (Dako), and sections were counterstained with Mayer's hematoxylin. For immunofluorescence, target antigens were revealed with specific secondary antibodies conjugated with fluorescent dyes (AlexaFluor; Thermo Fisher Scientific). Viral proteins were detected with a Tyramide signal amplification kit (Thermo Fisher Scientific) according to the manufacturer's protocol.

Neutralization Assays. The presence of neutralizing antibodies in infected and control sheep was assessed by microneutralization assays as previously described (3).

ELISPOT. Quantification of anti–ovalbumin-specific IgG-secreting cells by ELISPOT was carried out as previously described (43). Results were expressed as ASC number per 10^6 peripheral blood mononuclear cells (PBMCs).

ELISAs. Antigen-specific IgG and IgM were quantified in serum by indirect ELISA. Plates coated with recombinant VP7 protein were obtained from IDVet (ID Screen Bluetongue Milk Indirect) for the detection of αBTV antibodies (Abs). For the detection of αOVA Abs, ELISA plates (Maxisorp; Nunc) were coated with 2 μg OVA per well (Sigma-Aldrich). Antigen-specific Abs were revealed using secondary Abs directed against sheep IgG or IgM. Dilutions of a pool of positive control sera were included in each plate in duplicate to obtain a standard curve. Optical density (OD) values obtained from tested sera were interpolated with the standard curve and multiplied for the dilution factor to obtain the relative ELISA units.

Avidity Test. Antibody avidity was assessed by ELISA using the chaotropic agent ammonium thiocyanate (NH_4SCN) to dissociate low-affinity IgG binding using a previously described method (44, 45). An avidity index (AI) was calculated as the molar concentration of NH_4SCN required to reduce Ag-specific IgG binding by 50%.

Statistical Analyses. Nonparametric two-tailed Mann-Whitney rank *U* test, paired *t* test, and one-way ANOVA were used to compare treatment groups. Analyses were performed using Prism 6.0 (GraphPad).

ACKNOWLEDGMENTS. We thank Andrew Shaw, Meredith Stewart, Giovanni Di Guardo, and Clive McKimmie for critical reading of the manuscript. We also thank Berardo De Dominicis, Doriano Ferrari, Vincenzo D'Innocenzo, and Massimiliano Caporale for excellent animal handling and care. We are indebted to Luigina di Gialleonardo e Gianfranco Romeo for sample collection and processing. This study was funded by the Wellcome Trust (092806/Z/10/Z) and in part by a W.B. Martin Scholarship. Animal experiments conducted at the Istituto Zooprofilattico Sperimentale dell'Abruzzo e Molise "G. Caporale" were funded in part by the Italian Ministry of Health, whereas those in Centro de Investigación en Sanidad Animal were funded by Grants AGL2012-33289 (Ministerio de Economía y Competitividad) and S2013/ABI-2906 (Comunidad de Madrid-Fondo Europeo de Desarrollo Regional).

1. Weaver SC, Reisen WK (2010) Present and future arboviral threats. *Antiviral Res* 85(2):328–345.
2. Maclachlan NJ, Drew CP, Darpel KE, Worwa G (2009) The pathology and pathogenesis of bluetongue. *J Comp Pathol* 141(1):1–16.
3. Caporale M, et al. (2014) Virus and host factors affecting the clinical outcome of bluetongue virus infection. *J Virol* 88(18):10399–10411.
4. Darpel KE, et al. (2012) Involvement of the skin during bluetongue virus infection and replication in the ruminant host. *Vet Res (Faisalabad)* 43(1):40.
5. Mueller SN, Germain RN (2009) Stromal cell contributions to the homeostasis and functionality of the immune system. *Nat Rev Immunol* 9(9):618–629.
6. Jeggo MH, Wardley RC, Taylor WP (1984) Role of neutralising antibody in passive immunity to bluetongue infection. *Res Vet Sci* 36(1):81–86.
7. Pages N, et al. (2014) Culicoides midge bites modulate the host response and impact on bluetongue virus infection in sheep. *PLoS One* 9(1):e83683.
8. Diamond MS, Shrestha B, Marri A, Mahan D, Engle M (2003) B cells and antibody play critical roles in the immediate defense of disseminated infection by West Nile encephalitis virus. *J Virol* 77(4):2578–2586.
9. Burke DS, et al. (1985) Fatal outcome in Japanese encephalitis. *Am J Trop Med Hyg* 34(6):1203–1210.
10. Libraty DH, et al. (2002) Clinical and immunological risk factors for severe disease in Japanese encephalitis. *Trans R Soc Trop Med Hyg* 96(2):173–178.
11. Shepherd AJ, Swanepoel R, Leman PA (1989) Antibody response in Crimean-Congo hemorrhagic fever. *Clin Infect Dis* 11(Suppl 4):S801–S806.
12. Sánchez-Cordón PJ, et al. (2010) Immunohistochemical detection of bluetongue virus in fixed tissue. *J Comp Pathol* 143(1):20–28.
13. Girard J-P, Moussion C, Förster R (2012) HEVs, lymphatics and homeostatic immune cell trafficking in lymph nodes. *Nat Rev Immunol* 12(11):762–773.
14. Rantakari P, et al. (2015) The endothelial protein PLVAP in lymphatics controls the entry of lymphocytes and antigens into lymph nodes. *Nat Immunol* 16(4):386–396.
15. Junt T, et al. (2007) Subcapsular sinus macrophages in lymph nodes clear lymph-borne viruses and present them to antiviral B cells. *Nature* 450(7166):110–114.
16. Roozendaal R, et al. (2009) Conduits mediate transport of low-molecular-weight antigen to lymph node follicles. *Immunity* 30(2):264–276.

17. Gretz JE, Norbury CC, Anderson AO, Proudfoot AEI, Shaw S (2000) Lymph-borne chemokines and other low molecular weight molecules reach high endothelial venules via specialized conduits while a functional barrier limits access to the lymphocyte microenvironments in lymph node cortex. *J Exp Med* 192(10):1425–1440.
18. Wang X, et al. (2011) Follicular dendritic cells help establish follicle identity and promote B cell retention in germinal centers. *J Exp Med* 208(12):2497–2510.
19. Victora GD, Nussenzweig MC (2012) Germinal centers. *Annu Rev Immunol* 30: 429–457.
20. Janowicz A, et al. (2015) Multiple genome segments determine virulence of bluetongue virus serotype 8. *J Virol* 89(10):5238–5249.
21. Aguzzi A, Kranich J, Krautler NJ (2014) Follicular dendritic cells: Origin, phenotype, and function in health and disease. *Trends Immunol* 35(3):105–113.
22. Aydar Y, Sukumar S, Szakal AK, Tew JG (2005) The influence of immune complex-bearing follicular dendritic cells on the IgM response, Ig class switching, and production of high affinity IgG. *J Immunol* 174(9):5358–5366.
23. Kitamoto T, Muramoto T, Mohri S, Doh-Ura K, Tateishi J (1991) Abnormal isoform of prion protein accumulates in follicular dendritic cells in mice with Creutzfeldt-Jakob disease. *J Virol* 65(11):6292–6295.
24. Brown KL, et al. (1999) Scrapie replication in lymphoid tissues depends on prion protein-expressing follicular dendritic cells. *Nat Med* 5(11):1308–1312.
25. Burton GF, Keele BF, Estes JD, Thacker TC, Gartner S (2002) Follicular dendritic cell contributions to HIV pathogenesis. *Semin Immunol* 14(4):275–284.
26. Heesters BA, et al. (2015) Follicular Dendritic Cells Retain Infectious HIV in Cycling Endosomes. *PLoS Pathog* 11(12):e1005285.
27. Mackay F, Browning JL (1998) Turning off follicular dendritic cells. *Nature* 395(6697): 26–27.
28. Koni PA, Flavell RA (1999) Lymph node germinal centers form in the absence of follicular dendritic cell networks. *J Exp Med* 189(5):855–864.
29. Alimzhanov MB, et al. (1997) Abnormal development of secondary lymphoid tissues in lymphotoxin beta-deficient mice. *Proc Natl Acad Sci USA* 94(17):9302–9307.
30. Umeshappa CS, et al. (2011) A comparison of intradermal and intravenous inoculation of bluetongue virus serotype 23 in sheep for clinico-pathology, and viral and immune responses. *Vet Immunol Immunopathol* 141(3-4):230–238.
31. Pini A (1976) Study on the pathogenesis of bluetongue: Replication of the virus in the organs of infected sheep. *Onderstepoort J Vet Res* 43(4):159–164.
32. Barratt-Boyes SM, MacLachlan NJ (1994) Dynamics of viral spread in bluetongue virus infected calves. *Vet Microbiol* 40(3-4):361–371.
33. Hemati B, et al. (2009) Bluetongue virus targets conventional dendritic cells in skin lymph. *J Virol* 83(17):8789–8799.
34. Gretz JE, Kaldjian EP, Anderson AO, Shaw S (1996) Sophisticated strategies for information encounter in the lymph node: The reticular network as a conduit of soluble information and a highway for cell traffic. *J Immunol* 157(2):495–499.
35. Phan TG, Grigorova I, Okada T, Cyster JG (2007) Subcapsular encounter and complement-dependent transport of immune complexes by lymph node B cells. *Nat Immunol* 8(9):992–1000.
36. Carrasco YR, Batista FD (2007) B cells acquire particulate antigen in a macrophage-rich area at the boundary between the follicle and the subcapsular sinus of the lymph node. *Immunity* 27(1):160–171.
37. Jarjour M, et al. (2014) Fate mapping reveals origin and dynamics of lymph node follicular dendritic cells. *J Exp Med* 211(6):1109–1122.
38. Krautler NJ, et al. (2012) Follicular dendritic cells emerge from ubiquitous perivascular precursors. *Cell* 150(1):194–206.
39. Farr AG, Cho Y, De Bruyn PPH (1980) The structure of the sinus wall of the lymph node relative to its endocytic properties and transmural cell passage. *Am J Anat* 157(3): 265–284.
40. Phan TG, Green JA, Gray EE, Xu Y, Cyster JG (2009) Immune complex relay by subcapsular sinus macrophages and noncognate B cells drives antibody affinity maturation. *Nat Immunol* 10(7):786–793.
41. Gaya M, et al. (2015) Host response. Inflammation-induced disruption of SCS macrophages impairs B cell responses to secondary infection. *Science* 347(6222):667–672.
42. Arnaud F, et al. (2010) Interplay between ovine bone marrow stromal cell antigen 2/tetherin and endogenous retroviruses. *J Virol* 84(9):4415–4425.
43. Lefevre EA, Carr BV, Prentice H, Charleston B (2009) A quantitative assessment of primary and secondary immune responses in cattle using a B cell ELISPOT assay. *Vet Res* 40(1):3, 10.1051/vetres:2008041.
44. Pullen GR, Fitzgerald MG, Hosking CS (1986) Antibody avidity determination by ELISA using thiocyanate elution. *J Immunol Methods* 86(1):83–87.
45. Nair N, et al. (2007) Age-dependent differences in IgG isotype and avidity induced by measles vaccine received during the first year of life. *J Infect Dis* 196(9):1339–1345.